

Input Convex Kolmogorov Arnold Networks

Thomas DESCHATRE*

Xavier WARIN †

January 15, 2026

Abstract

This article presents an input convex neural network architecture using Kolmogorov-Arnold networks (ICKAN). Two specific networks are presented: the first is based on a low-order, linear-by-part, representation of functions, and a universal approximation theorem is provided. The second is based on cubic splines, for which only numerical results support convergence. We demonstrate on simple tests that these networks perform competitively with classical input convex neural networks (ICNNs). In a second part, we use the networks to solve some optimal transport problems needing a convex approximation of functions and demonstrate their effectiveness. Cubic ICKANs produce results similar to those of classical ICNNs.

1 Introduction

Recently, Kolmogorov-Arnold Networks (KANs) have been introduced as an alternative to multilayer perceptrons for high-dimensional function approximation, based on the Arnold-Kolmogorov representation theorem [20]. Arnold and Kolmogorov demonstrated [15] that a multivariate continuous smooth \mathbb{R} valued function f on a bounded domain can be expressed as a finite composition of sums of continuous single-variable functions. Specifically, if f is continuous on $[0, 1]^n$, then

$$f(x) = \sum_{i=1}^{2n+1} \psi_i \left(\sum_{j=1}^n \Phi_{i,j}(x_j) \right), \quad (1)$$

where $\Phi_{i,j} : [0, 1] \rightarrow \mathbb{R}$ and $\psi_i : \mathbb{R} \rightarrow \mathbb{R}$, $i = 1, \dots, 2n + 1$, $j = 1, \dots, n$. Since one-dimensional functions ψ and Φ can be highly irregular or even fractal, it has been demonstrated that they may not be practically learnable [13, 25]. To address this issue, Kůrková in [18, Theorem 1] considered an approximate representation f_m instead of an exact one for a continuous function f , also extending the outer sum to m terms instead of $2n + 1$, m being intended to be large and greater than $2n + 1$. More recently, under the assumption that f is α -Hölder ($0 < \alpha < 1$) and also using m terms on the outer summation, [29] constructed an approximation f_m with $\Phi_{i,j} \in C^2$ converging to f in the sup norm as m increases (see also [9] for another construction approximating the function in the sup norm). In this work, we follow the approach of [20]. Firstly, they suggest not limiting the outer sum in (1) to $2n + 1$ terms but to m terms and define a KAN l^{th} layer, $l =$

*EDF R&D & FiME thomas.deschatre at edf.fr

†EDF R&D & FiME xavier.warin at edf.fr

$0, \dots, L$, as an operator $\psi_{m,q}^l$ from $[0, 1]^m$ to \mathbb{R}^q :

$$(\psi_{m,q}^l(x))_k = \sum_{j=1}^m \Phi_{l,k,j}(x_j), \text{ for } k = 1, \dots, q. \quad (2)$$

Second, by stacking the layers, i.e., composing the operators ψ^l , $l = 0 \dots, L$, they define the KAN operator from $[0, 1]^m$ to \mathbb{R} :

$$K(x) = \psi_{n_{L-1},d}^L \circ \psi_{n_{L-2},n_{L-1}}^{L-1} \circ \dots \circ \psi_{n_0,n_1}^1 \circ \psi_{m,n_0}^0(x). \quad (3)$$

Since all ψ functions are one-dimensional, many classical methods are available to propose an easy-to-implement approximation. The original implementation proposed in [20] uses B-Splines and is numerically costly but many other approximations based on wavelets [4], radial basis [19, 30], Chebyshev polynomials [28] have been proposed to decrease this computing time. All of these representations suffer from the same theoretical flaw: the output of a layer may not be in the grid initially chosen for the following layer. Sending back the output of a layer, a priori in \mathbb{R}^q to $[0, 1]^q$ using, for example, a sigmoid function is possible. However, the observed convergence pace degrades. Aware of this problem, [20] proposes an adaptation technique, but this approach numerically fails. Recently, using a P1 finite element flavour, [35] proposes a new architecture P1-KAN avoiding this flaw and proves its convergence : numerical examples based on function approximation using a mean squared error (MSE) criterion or real applications optimizing hydraulic valleys have shown that the P1-KAN is more effective than MLP and all tested KANs.

In this article, we extend the work of [35] and propose new architectures to approximate convex functions with a convex approximation. The convexity of the functions that we want to approximate is essential in many applications. For example, in optimal transport, the optimal transport map is the gradient of a convex function, as stated in Brenier’s theorem [5]. Similarly, in optimal control, the value function that we want to optimize can be convex or concave. For example, when optimizing gas storage, it is very important for practitioners to maintain the concavity of the Bellman values with respect to the stock level. The marginal cost, which is defined as the derivative of these Bellman values with respect to the stock level, must decrease as the stock level increases. The approximation of a convex function while preserving its convexity property has been investigated in many articles. The approximation by cuts of a convex function using regression methods has been studied in [3, 11, 12] and [14], leading to max-affine approximations. A max-affine representation using group-max neural networks [34] has been proposed and proven to be convergent relying on the fact that a convex function can be ϵ approximated by the maximum of a set a affine functions. The theoretical investigation of convex function approximation has also recently been explored, as demonstrated in [6], using a one-layer feedforward neural network with exponential activation functions in the inner layer and a logarithmic activation at the output known as the log-sum-exp function, a standard convex function that appears in logistic regression. Numerically, this issue has been addressed in [2] through the development of the Input Convex Neural Network (ICNN) methodology, which is proven to be convergent in [7]. This effective approach has been widely applied in various fields requiring convex approximation, such as optimal transport problems [21, 16], optimal control problems [7, 1], inverse problems [24], and general optimization problems [8], among others. Input convex networks based on the original Kolmogorov-Arnold network have also recently been tested for modelling hyperelastic materials in [31], concomitant to our work.

We propose two Kolmogorov-Arnold Networks:

- The first version is based on a piecewise linear approximation of the 1D functions involved in the KAN approximation. It is based on the P1-KAN network recently developed in [35]. Different from other

KAN networks, it inputs a grid G^1 defining the approximation domain and outputs a function value f approximating the data and a grid G^2 defining the image of the initial grid G^1 by f . This clear definition of a layer allows us to compose the layers easily. Imposing convexity in the one dimensional approximation, we develop a new network and we provide a Universal Approximation Theorem.

- The second one is based on the Hermite cubic-spline approximation where convexity is also imposed. This network enables us to provide a high-order approximation of a function, which can be a desired feature, for example, when the gradient of the convex approximation is the target. In this case a piecewise linear approximation provides a constant per mesh approximation which is not sufficient enough. However, no convergence property is given.

In (2), we describe the two networks belonging to the class of Input Convex Kolmogorov Networks (ICKAN), giving two variants, whether the grid is adapted or not, as in [35]. The different variations are tested using a mean squared error criterion, and we show that we can achieve results comparable to the best ones obtained by ICNNs.

In (3), we extend the previous networks to the case where the function to approximate is only partially convex with respect to the input, leading to Partial Input Convex Kolmogorov Networks (PICKAN). We again provide results comparing the efficiency of the PICKANs to the partial convex version of ICNNs (PICNN).

In (4), we use ICKANs to estimate the optimal transport map between two distributions μ and ν using the Wasserstein distance $W_2(\mu, \nu)$ on simulated data, showing the efficiency of the proposed networks.

2 ICKAN

We suppose here that the function to approximate is fully convex. In a first part we explain how to derive a one dimensional convex approximation of a function on $[0, 1]$ either using a piecewise linear approximation or a cubic-spline one. We show in (A) that adapting meshes can be an interesting feature on a numerical example. In a second part, we detail the different layers construction with the two networks and provide a Universal Approximation Theorem for the first network. In a third part, numerical examples are given.

2.1 Approximation of a 1D convex function f on $[0, 1]$

We introduce the lattice $\{\hat{x}_0 := 0\} \cup (\hat{x}_p)_{1 \leq p \leq P-1} \cup \{\hat{x}_P := 1\}$ where the \hat{x}_p in $[0, 1]$ are increasing values with p .

2.1.1 Piecewise linear approximation

For $P > 0$, the degrees of freedom of a $P1$ approximation ϕ of f are the values of the function on the lattice leading to

$$\phi(x) = \sum_{p=0}^P a_p \Psi_p(x) \quad (4)$$

where $(a_p)_{p=0, \dots, P}$ are approximations of $(f(\hat{x}_p))_{p=0, \dots, P}$ and $(\Psi_p)_{p=0, \dots, P}$ is the basis of the shape functions: these functions have compact support in each interval $[\hat{x}_{p-1}, \hat{x}_{p+1}]$ for $p = 1, \dots, P-1$ and are defined as:

$$\Psi_p(x) = \begin{cases} \frac{x - \hat{x}_{p-1}}{\hat{x}_p - \hat{x}_{p-1}} & \text{for } x \in [\hat{x}_{p-1}, \hat{x}_p], \\ \frac{\hat{x}_{p+1} - x}{\hat{x}_{p+1} - \hat{x}_p} & \text{for } x \in [\hat{x}_p, \hat{x}_{p+1}], \end{cases} \quad (5)$$

for $p = 1, \dots, P-1$ and $\Psi_0(x) = \max(1 - \frac{x - \hat{x}_0}{\hat{x}_1 - \hat{x}_0}, 0)$, $\Psi_P(x) = \max(\frac{x - \hat{x}_{P-1}}{\hat{x}_P - \hat{x}_{P-1}}, 0)$ (see (1)). As we are interested

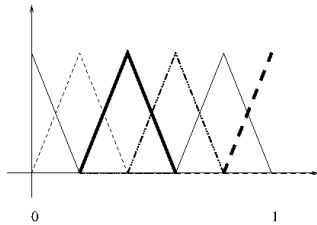


Figure 1: Uniform P1 basis functions on $[0, 1]$ with $P = 5$.

in having a convex function, we want our piecewise linear approximation to have increasing derivatives with x on each mesh $[\hat{x}_p, \hat{x}_{p+1}]$ for $p = 0, \dots, P-1$. The trainable variables of the convex approximation are b , an approximation of $f(0)$, \hat{b} , an approximation of $f'(0)$, and $(d_i)_{i=1, \dots, P-1}$ an approximation of $f'(\hat{x}_i) - f'(\hat{x}_{i-1})$ for $i = 1, \dots, P$.

Therefore $a_p \approx f(\hat{x}_p)$ in (4) is given by:

$$a_p = b + \sum_{j=1}^p \left(\hat{b} + \sum_{i=1}^{j-1} \max(d_i, 0) \right) (\hat{x}_j - \hat{x}_{j-1}), \quad p = 0, \dots, P, \quad (6)$$

where the max is here to ensure that the approximation $f'(\hat{x}_p) \approx \hat{b} + \sum_{i=1}^p \max(d_i, 0)$ is increasing with p .

It is also possible to adapt the grid as in [35]. In that case, the vertices in $]0, 1[$ are initially generated randomly uniformly and their values are trained to adapt to the data. This is done by defining for $1 \leq p < P$ increasing values in $]0, 1[$ by

$$\hat{x}_p = \frac{\sum_{k=1}^p e_k}{\sum_{k=1}^P e_k}, \quad (7)$$

where e_1, \dots, e_P are positive variables. Therefore, $b, \hat{b}, (d_i)_{i=1, \dots, P-1}$ and $(e_i)_{i=1, \dots, P}$ are trained by the algorithm. In (A.1), we demonstrate the effect of adaptation for the P1-ICKAN.

2.1.2 The cubic approximation

On a mesh $[\hat{x}_p, \hat{x}_{p+1}]$, the function f is approximated for $x \in [\hat{x}_p, \hat{x}_{p+1}]$ using a cubic Hermite spline by $\phi_p \left(\frac{x - \hat{x}_p}{\hat{x}_{p+1} - \hat{x}_p} \right)$ with:

$$\begin{aligned} \phi_p(t) = & f(\hat{x}_p)h_{00}(t) + f'(\hat{x}_p)h_{10}(t)(\hat{x}_{p+1} - \hat{x}_p) \\ & + f(\hat{x}_{p+1})h_{01}(t) + f'(\hat{x}_{p+1})h_{11}(t)(\hat{x}_{p+1} - \hat{x}_p) \end{aligned}$$

and

$$\begin{aligned} h_{00}(t) &= 2t^3 - 3t^2 + 1, \\ h_{10}(t) &= t^3 - 2t^2 + t, \\ h_{01}(t) &= -2t^3 + 3t^2, \\ h_{11}(t) &= t^3 - t^2. \end{aligned}$$

As previously we require that the derivatives are increasing. Under this condition, in order to get a convex approximation, we can check that the values $\{f(\hat{x}_p)\}_{p=0,\dots,P}$ have to satisfy for $p = 0, \dots, P - 1$:

$$\begin{aligned} f(\hat{x}_p) + \frac{\hat{x}_{p+1} - \hat{x}_p}{3} \left(2f'(\hat{x}_p) + f'(\hat{x}_{p+1}) \right) &\leq f(\hat{x}_{p+1}), \\ f(\hat{x}_{p+1}) &\leq f(\hat{x}_p) + \frac{\hat{x}_{p+1} - \hat{x}_p}{3} \left(f'(\hat{x}_p) + 2f'(\hat{x}_{p+1}) \right). \end{aligned}$$

Therefore the convex approximation based on Cubic spline is defined on mesh $[\hat{x}_p, \hat{x}_{p+1}]$ for $p = 0, \dots, P - 1$ by $\phi_p \left(\frac{x - \hat{x}_p}{\hat{x}_{p+1} - \hat{x}_p} \right)$ with

$$\phi_p(t) = a_p^0 h_{00}(t) + a_p^1 h_{10}(t)(\hat{x}_{p+1} - \hat{x}_p) + a_{p+1}^0 h_{01}(t) + a_{p+1}^1 h_{11}(t)(\hat{x}_{p+1} - \hat{x}_p), \quad (8)$$

with :

$$\begin{aligned} a_p^1 &= \hat{b} + \sum_{i=1}^p \max(d_i, 0), \\ a_p^0 &= b + \sum_{i=1}^p \frac{\hat{x}_i - \hat{x}_{i-1}}{3} \left(2a_{i-1}^1 + a_i^1 + \sigma(g_i)(a_i^1 - a_{i-1}^1) \right), \end{aligned} \quad (9)$$

σ the sigmoid function and $\hat{b}, b, \{d_i\}_{i=1,\dots,p}, \{g_i\}_{i=1,\dots,p}$ are trainable. In the adapted version, $(e_i)_{i=1,\dots,P}$ are also trained. In (A.2), we demonstrate the effect of the adaptation of Cubic-ICKAN and the effect of optimizing one layer.

2.2 The ICKAN layers

As for the P1-KAN layer, an ICKAN layer inputs an hypercube defining the domain and the x batched values, and it outputs an estimation of the function at x and an hypercube defined by the image of the initial hypercube. This allow us to concatenate the different layers in a coherent way.

2.2.1 The P1-ICKAN layers

As the first component of the first layer, we define $\hat{\kappa}_{n,m}^0$ for $x \in [0, 1]^n$ and the hypercube $G^0 := [0, 1]^n$ as:

$$\begin{aligned} \hat{\kappa}_{n,m}^0(x, G^0)_k &= \\ \sum_{j=1}^n \sum_{p=0}^P \left(b_{0,k,j} + \sum_{s=1}^p \left(\hat{b}_{0,k,j} + \sum_{i=1}^{s-1} \max(d_{0,k,j,i}, 0) \right) (\hat{x}_{0,j,s} - \hat{x}_{0,j,s-1}) \right) \Psi_p^{0,j}(x_j), & (10) \\ \text{for } k &= 1, \dots, m, \end{aligned}$$

where the $(\hat{x}_{0,j,s})_{s=0,\dots,P}$ correspond to the one dimensional lattice of the j^{th} dimension of G^0 and the $\Psi_p^{0,j}$ to the functions defined in (5) and displayed in (1).

The image $G^1 = \prod_{k=1}^m [\underline{G}_k^1, \bar{G}_k^1]$ of G^0 by $\hat{\kappa}_{n,m}^0$ is exactly given by:

$$\begin{aligned}\underline{G}_k^1 &= \sum_{j=1}^n \min_{0 \leq p \leq P} \left[b_{0,k,j} + \sum_{s=1}^p \left(\hat{b}_{0,k,j} + \sum_{i=1}^{s-1} \max(d_{0,k,j,i}, 0) \right) (\hat{x}_{0,j,s} - \hat{x}_{0,j,s-1}) \right] \\ \bar{G}_k^1 &= \sum_{j=1}^n \max \left[b_{0,k,j}, b_{0,k,j} + \sum_{s=1}^P \left(\hat{b}_{0,k,j} + \sum_{i=1}^{s-1} \max(d_{0,k,j,i}, 0) \right) (\hat{x}_{0,j,s} - \hat{x}_{0,j,s-1}) \right]\end{aligned}\quad (11)$$

for $1 \leq k \leq m$, and the layer is defined as

$$\kappa_{n,m}^0(x, G^0) = (\hat{\kappa}_{n,m}^0(x, G^0), G^1). \quad (12)$$

remark 2.1 *As the approximation is convex, we have used the fact that the maximum \bar{G}_k^1 is reached on the boundary of the domain.*

As a sum of convex 1D functions in each dimension, the Hessian of $\hat{\kappa}_{n,m}^0(\cdot, G^0)$ is diagonal and definite positive.

As the first layer is convex in x , it remains to ensure that it remains convex in x by composition of a layer $\hat{\kappa}_{m,q}^l(\cdot, G^l)$. As in [2], it is sufficient to have for $l \geq 1$, $\hat{\kappa}_{m,q}^l(x, G^l)_k$ convex and increasing in x and naturally we only have to impose that $\hat{b}_{l,k,j} \geq 0$ for all k and j . Therefore for $l \geq 1$, G^l being the hypercube defining the domain, we first define

$$\begin{aligned}\hat{\kappa}_{m,q}^l(x, G^l)_k &= \\ & \sum_{j=1}^m \sum_{p=0}^P \left(b_{l,k,j} + \sum_{s=1}^p \left(\max(\hat{b}_{l,k,j}, 0) + \sum_{i=1}^{s-1} \max(d_{l,k,j,i}, 0) \right) (\hat{x}_{l,j,s} - \hat{x}_{l,j,s-1}) \right) \Psi_p^{l,j}(x_j), \\ & \text{for } k = 1, \dots, q,\end{aligned}$$

and the output hypercube G^{l+1} image of G^l is given by an expression similar to (11). Then the layer is defined by:

$$\kappa_{m,q}^l(x, G^l) = (\hat{\kappa}_{m,q}^l(x, G^l), G^{l+1}). \quad (13)$$

Concatenating the L layers, noting n_l the number of neurons of layer l (see (3)), supposing the number of mesh points P constant from one neuron to another, we define our global network as

$$K(x) = \hat{\kappa}_{n_{L-1},1}^L \circ \kappa_{n_{L-2},n_{L-1}}^{L-1} \circ \dots \circ \kappa_{n_0,n_0}^0(x, [0, 1]^n). \quad (14)$$

As in [35], we propose two versions:

- A first version, setting the lattice using a uniform meshing and the trainable variables are

$$\begin{aligned}\mathcal{A} &:= (b_{0,k,j}, \hat{b}_{0,k,j}, (d_{0,k,j,i})_{i=1,\dots,P-1})_{k=1,\dots,n_0, j=0,\dots,n} \cup \\ & (b_{l,k,j}, \hat{b}_{l,k,j}, (d_{l,k,j,i})_{i=1,\dots,P-1})_{l=1,\dots,L-1, k=1,\dots,n_l, j=0,\dots,n_{l-1}} \cup \\ & (b_{L,1,j}, \hat{b}_{L,1,j}, (d_{L,1,j,i})_{i=1,\dots,P-1})_{j=0,\dots,n_{L-1}}.\end{aligned}$$

- A second version also trains the lattice values inside the domain and the trainable variables become

$$\mathcal{A} \cup (e_{0,j,p})_{j=1,\dots,n, p=1,\dots,P} \cup (e_{l,j,p})_{l=1,\dots,L, j=1,\dots,n_l, p=1,\dots,P}$$

where the $e_{l,j,p}$ are used to defined the $\hat{x}_{l,j,p}$ using an equation similar to (7).

2.2.2 The Cubic-ICKAN layers

Consider again $(\hat{x}_{0,j,s})_{s=0,\dots,P}$ the one dimensional lattice on $G^0 := [0, 1]^n$ of the j^{th} dimension input. We define $\hat{\kappa}_{n,m}^0$ for $x \in \prod_{j=1}^n [\hat{x}_{0,j,p_j}, \hat{x}_{0,j,p_j+1}]$ where $p_j \in \{0, \dots, P-1\}$ for $j = 1, \dots, n$ and the hypercube G^0 by

$$\begin{aligned} \hat{\kappa}_{n,m}^0(x, G^0)_k &= \sum_{j=1}^n a_{0,j,p_j}^0 h_{00}(t_{0,j}) + a_{0,j,p_j}^1 h_{10}(t_{0,j})(\hat{x}_{0,j,p_j+1} - \hat{x}_{0,j,p_j}) \\ &\quad + a_{0,j,p_j+1}^0 h_{01}(t_{0,j}) + a_{0,j,p_j+1}^1 h_{11}(t_{0,j})(\hat{x}_{0,j,p_j+1} - \hat{x}_{0,j,p_j}), \\ &\quad \text{for } k = 1, \dots, m, \end{aligned} \tag{15}$$

where $t_{0,j} = \frac{x_j - \hat{x}_{0,j,p_j}}{\hat{x}_{0,j,p_j+1} - \hat{x}_{0,j,p_j}}$,

$$\begin{aligned} a_{0,j,p_j}^1 &= \hat{b}_{0,j} + \sum_{i=1}^{p_j} \max(d_{0,j,i}, 0), \\ a_{0,j,p_j}^0 &= b_{0,j} + \sum_{i=1}^{p_j} \frac{\hat{x}_{0,j,i} - \hat{x}_{0,j,i-1}}{3} (2a_{0,j,i}^1 + a_{0,j,i-1}^1 + \sigma(g_{0,j,i})(a_{0,j,i}^1 - a_{0,j,i-1}^1)). \end{aligned} \tag{16}$$

$G^1 = \prod_{k=1}^m [\underline{G}_k^1, \bar{G}_k^1]$ defined with

$$\begin{aligned} \underline{G}_k^1 &= \sum_{j=1}^n \min_{0 \leq p \leq P} a_{0,j,p}^0 \\ \bar{G}_k^1 &= \sum_{j=1}^{d_0} \max [a_{0,j,0}^0, a_{0,j,P}^0], \end{aligned} \tag{17}$$

is now included in the image of G^0 . In order that G^1 is exactly the image of G^0 , we can truncate the output of the layer $\hat{\kappa}$ and :

$$\kappa_{n,m}^0(x, G^0) = \left(\left(\max(\hat{\kappa}_{n,m}^0(x, G^0)_k, \underline{G}_k^1) \right)_{k=1,\dots,m}, G^1 \right).$$

remark 2.2 *Due to convexity, only the minimum value needs to be truncated. Clipping the value function reveals the image of the layer, which defines a grid that can serve as input for another layer. Using semi-Lagrangian schemes for control problems and clipping solution values while using Lagrange interpolators defines a nearly monotone scheme and permits to get convergence rates [33]. The original KAN defines layers without adapting the grid size to the output domain of the preceding layer, yet it is known to produce excellent results. Therefore, truncation may not be compulsory, and numerical tests have shown that its effect is minimal.*

Similarly to the piecewise linear case, for $l \geq 1$, G^l being the hypercube defining the domain, the operator $\hat{\kappa}_{m,q}^l(x, G^l)_k$ for $l \geq 1$ is defined similarly to (15) using

$$a_{l,j,p_j}^1 = \max(\hat{b}_{l,j}, 0) + \sum_{i=1}^{p_j} \max(d_{l,j,i}, 0)$$

instead of (16). The output hypercube G^{l+1} image of G^l is given by an expression similar to (17). Then the layer is defined by:

$$\kappa_{m,q}^l(x, G^l) = \left(\left(\max(\hat{\kappa}_{m,q}^l(x, G^l)_k, \underline{G}_k^{l+1}) \right)_{k=1, \dots, q}, G^{l+1} \right).$$

The concatenation of the layers is still given by (14). As for the piecewise linear case, we can either use a uniform meshing or adapting one.

2.2.3 Convergence results

We provide two universal approximation theorems in the piecewise linear case for the two different cases, adapted and non adapted.

Theorem 2.1 *The space spanned by the P1-ICKAN letting n_l for $l = 0, \dots, L - 1$ and L vary for $P > 1$ is dense in the set of Lipschitz convex functions on $[0, 1]^n$ with the sup norm when adaptation is used.*

The proof of (2.1) is given in (B.1). We give at last a theorem for the non adapted case, with proof in (B.2).

Theorem 2.2 *The space spanned by the P1-ICKAN letting n_l for $l = 0, \dots, L - 1$, L and P vary is dense in set of Lipschitz convex functions on $[0, 1]^n$ with the sup norm when no adaptation is used.*

2.2.4 Numerical Results

In this section, we compare the performance of different networks to that of the ICNN. First, we consider the approximation performance on a d-dimensional convex function, and then we study a two-dimensional toy control example.

Numerical approximation We estimate the function

$$f(x) = \sum_{i=1}^d (|x_i| + |1 - x_i|) + x^\top Ax \tag{18}$$

where A is a positive definite matrix using an Input Convex Neural Network with a ReLU activation function and an Input Convex Kolmogorov Network approximation \tilde{f}^θ parametrized by θ by minimizing the empirical version of

$$\mathbb{E}[(f(X) - \tilde{f}^\theta(X))^2] \tag{19}$$

where $X \sim U[-2, 2]^d$. We use ADAM optimizer with a learning rate equal to 10^{-3} , a batch size equal to 1000 and use 200000 iterations. Using 10 runs, the average MSE with a batch of 100000 and its standard deviation are computed with different parametrizations. For the ICNN, we use 2, 3, 4 or 5 layers, a number of neurons in $\{10, 20, 40, 80, 160, 320\}$ and the ReLU activation function. Testing all configurations, our ICNN reference is the one with the smallest averaged MSE. Results are given in (1) and (2) in dimensions 3 and 7. Results with the P1-ICKAN are stable with the number of layers, and P . Results with adaptation (P1-ICKAN adapt) are better than without adaptation (P1-ICKAN). The P1-ICKAN with adaptation gives results similar to the best ICNN in dimension 3 and better than the best ICNN in dimension 7, while using a smaller network. Interestingly, the computational cost is rather independent of P and the dimension of the problem: this is due to the effective parallelization on GPU. The P1-ICKAN needs less parameters than the feedforward but the computational is between 3 and 4 times higher.

Table 1: Results on 10 runs on the minimization of (19) in dimension 3 with function in (18) : ICCN versus P1-ICKAN. *NBL* stands for the number of layers, *NBN* the number of neurons, *nbParam* the number of parameters of the model, while *Time* stands for the time in seconds for one hundred iterations of the stochastic gradient.

method	NBL	NBN	P	Average	std	nbParam	Time
Best ICNN	2	320		9.37E-05	8.29E-05	105284	0.14
P1-ICKAN	2	20	20	1.56E-04	7.39E-05	10080	0.54
P1-ICKAN	2	20	40	1.14E-04	9.79E-05	19680	0.54
P1-ICKAN	2	40	20	2.62E-04	3.68E-04	36960	0.55
P1-ICKAN	2	40	40	2.69E-04	4.65E-04	72160	0.53
P1-ICKAN	3	20	20	3.13E-04	3.10E-04	18480	0.73
P1-ICKAN	3	20	40	6.83E-04	1.04E-03	36080	0.73
P1-ICKAN	3	40	20	2.76E-04	1.90E-04	70560	0.73
P1-ICKAN	3	40	40	1.67E-04	2.91E-04	137760	0.73
P1-ICKAN adapt	2	20	20	1.23E-04	4.62E-05	10940	0.66
P1-ICKAN adapt	2	20	40	1.93E-04	3.72E-04	21400	0.66
P1-ICKAN adapt	2	40	20	2.62E-04	2.97E-04	38620	0.66
P1-ICKAN adapt	2	40	40	1.13E-04	1.42E-04	75480	0.66
P1-ICKAN adapt	3	20	20	9.82E-04	2.23E-03	19740	0.88
P1-ICKAN adapt	3	20	40	1.93E-04	2.75E-04	38600	0.88
P1-ICKAN adapt	3	40	20	3.63E-04	6.50E-04	73020	0.88
P1-ICKAN adapt	3	40	40	5.35E-04	1.16E-03	142680	0.88

Table 2: Results on 10 runs on the minimization of (19) in dimension 7 with function in (18): ICCN versus P1-ICKAN. *NBL* stands for the number of layers, *NBN* the number of neurons, *nbParam* the number of parameters of the model, while *Time* stands for the time in seconds for one hundred iterations of the stochastic gradient.

method	NBL	NBN	P	Average	std	nbParam	Time
Best ICNN	2	320		2.39E-03	6.72E-04	107848	0.14
P1-ICKAN	2	40	10	8.19E-03	9.23E-04	21120	0.54
P1-ICKAN	2	40	20	3.71E-03	4.69E-03	40320	0.54
P1-ICKAN	2	40	40	1.94E-03	1.20E-03	78720	0.53
P1-ICKAN	3	40	10	9.05E-03	1.25E-03	38720	0.73
P1-ICKAN	3	40	20	2.40E-03	8.88E-04	73920	0.73
P1-ICKAN	3	40	40	3.45E-03	2.09E-03	144320	0.73
P1-ICKAN adapt	2	40	10	2.31E-03	6.88E-04	21990	0.66
P1-ICKAN adapt	2	40	20	2.72E-03	2.95E-03	42060	0.67
P1-ICKAN adapt	2	40	40	1.33E-03	1.03E-03	82200	0.67
P1-ICKAN adapt	3	40	10	2.69E-03	1.08E-03	39990	0.88
P1-ICKAN adapt	3	40	20	2.87E-03	1.89E-03	76460	0.89
P1-ICKAN adapt	3	40	40	2.24E-03	2.47E-03	149400	0.89

Table 3: Results on 10 runs on the minimization of (19) in dimension 7 with function in (18): ICCN versus Cubic-ICKAN (C-ICKAN). *NBL* stands for the number of layers, *NBN* the number of neurons, *nbParam* the number of parameters of the model, while *Time* stands for the time in seconds for one hundred iterations of the stochastic gradient.

method	NBL	NBN	P	Average	std	nbParam	Time
Best ICNN	2	320		2.39E-03	6.72E-04	107848	0.14
C-ICKAN	2	20	10	6.66E-03	2.06E-03	12320	1.32
C-ICKAN	2	20	20	3.59E-03	7.64E-04	23520	1.31
C-ICKAN	2	40	10	3.88E-03	1.06E-03	42240	1.47
C-ICKAN	3	20	10	6.19E-03	2.11E-03	21120	1.79
C-ICKAN	3	20	20	5.04E-03	2.81E-03	40320	1.79
C-ICKAN	3	40	10	3.82E-03	1.64E-03	77440	2.03
C-ICKAN adapt	2	20	10	1.43E-03	6.29E-04	12790	1.49
C-ICKAN adapt	2	20	20	1.19E-03	8.76E-04	24460	1.55
C-ICKAN adapt	2	40	10	1.38E-03	1.28E-03	43110	1.65
C-ICKAN adapt	3	20	10	3.06E-03	1.66E-03	21790	2.06
C-ICKAN adapt	3	20	20	1.95E-03	1.43E-03	41660	2.07
C-ICKAN adapt	3	40	10	1.49E-03	1.11E-03	78710	2.23

In (3), results in dimension 7 using the Cubic-ICKAN show that the approximation is good but at a computational cost much higher than the P1-ICKAN.

We may wonder what would happen if we incorrectly assumed that the function to be evaluated was convex. We take

$$f(x) = A + 2\mathbf{1}_d^\top x + x^\top Qx, \quad (20)$$

with $Q = -0.5$ if $d = 1$, $Q = \begin{pmatrix} 1 & 0 \\ 0 & -0.5 \end{pmatrix}$ if $d = 2$, and $\mathbf{1}_d$ the vector of dimension d with all components equal to 1. (2) and (3) show that the error is concentrated on the axis supporting the convexity : the quadratic shape of the error indicates that the network is clipping the negative eigenvalues of the hessian matrix.

A toy control example in dimension 2 We consider the simple linear quadratic problem with dynamics

$$x_{t+1} = Ax_t + Bu_t + w_t, \text{ for } t = 0, \dots, N - 1,$$

where $(x_t, u_t, w_t) \in \mathbb{R}^2 \times \mathbb{R}^2 \times \mathbb{R}^2$, $(w_t)_{t=0, \dots, N-1}$ are identically and independently distributed centered gaussian noises with variance $W \in \mathbb{R}^{2 \times 2}$. The control $u_t = \phi_t(x_t)$ is taken in feedback form before discovering the noise and the initial value x_0 is given ; $A, B \in \mathbb{R}^{2 \times 2}$. The objective function to minimize is given by

$$J(x_0) = \mathbb{E} \left[\sum_{t=0}^{N-1} x_t^\top Qx_t + u_t^\top Ru_t + x_N^\top Q_f x_N | x_0 \right]$$

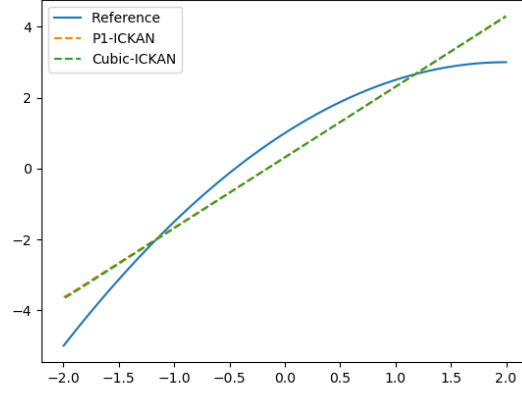


Figure 2: Estimation of the function (20) in dimension 1 wrongly supposing that the function is convex, network with $P = 10$.

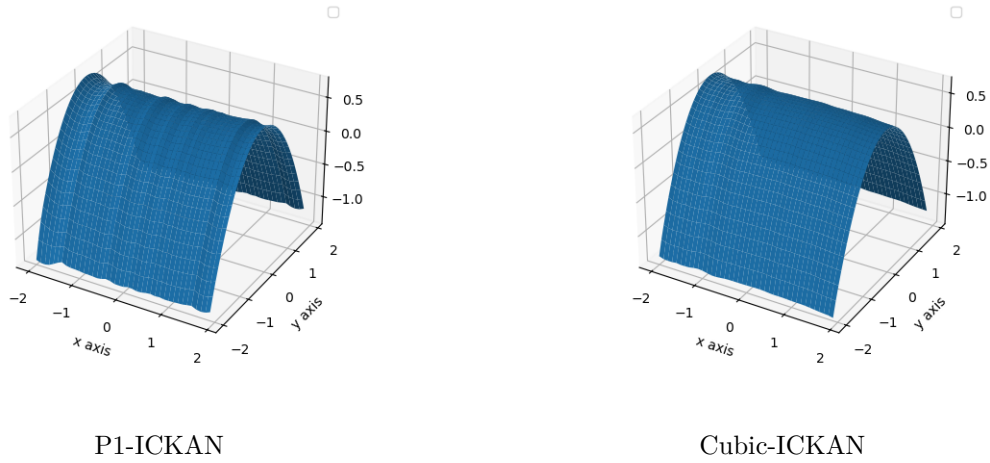


Figure 3: Error in dimension 2 for the function (20) wrongly supposing that the function is convex, network with $P = 10$.

where Q and R are 2 positive 2 dimensional matrices.
The optimal control is given by

$$\begin{aligned}\phi_t(x_t) &= K_t x_t, \\ K_t &= -(B^\top P_{t+1} B + R)^{-1} B^\top P_{t+1} A,\end{aligned}$$

where

$$\begin{aligned}P_t &= A^\top P_{t+1} A - A^\top P_{t+1} B (B^\top P_{t+1} B + R)^{-1} B^\top P_{t+1} A + Q \\ P_N &= Q_f\end{aligned}$$

and $J(x_0) = x_0^\top P_0 x_0 + r_0$ with

$$\begin{aligned}r_t &= r_{t+1} + \text{Tr}[W P_{t+1}] \\ r_N &= 0.\end{aligned}$$

We suppose that the optimal control u^* is exactly known and we want to calculate the convex value function J for $x_0 \in [-3, 3]^2$.

Applying the optimal control for a realization of $(w_t)_{t=0, \dots, N-1}$ and $x_0 \in U([-3, 3]^2)$ we get a cost

$$C(x_0, (w_t)_{t=0, \dots, N-1}) = \sum_{t=0}^{N-1} (x_t)^\top Q x_t + (K_t x_t)^\top R (K_t x_t) + x_N^\top Q_f x_N$$

so that with using a convex neural network κ^θ parametrized by θ to estimate J , we minimize on θ :

$$L(\theta) = \mathbb{E}[(\kappa^\theta(x_0) - C(x_0, (w_t)_{t=0, \dots, N-1}))^2] \quad (21)$$

We consider the parameters $Q = R = A = B = Q_f = W = \begin{pmatrix} 1 & 1 \\ 1 & 1 \end{pmatrix}$. In the numerical test, we take the same parameters for the optimizer as in the previous section. For the ICNN, we take 3 hidden layers with 30 neurons, while with the ICKAN we take 2 hidden layers of 10 neurons and $P = 10$. One hundred iterations of the stochastic gradient take 0.29 seconds with the ICNN, 0.69 seconds with the P1-ICKan and 1.14 seconds with the Cubic-ICKAN.

On (4) we plot the relative errors obtained by the three networks. The maximal error is nearly divided by two using the convex KAN networks. As expected, the Cubic network gives a smoother representation.

3 PICKAN

We suppose in this section that the function f to approximate is partially convex : $f(x, y)$ is convex in $y \in \mathbb{R}^{n_y}$ but not convex in $x \in \mathbb{R}^{n_x}$. We suppose that the function is defined on $G^0 = G_x^0 \times G_y^0$ where $G_x^0 = [0, 1]^{n_x}$, $G_y^0 = [0, 1]^{n_y}$. We only present the network using a piecewise linear approximation of a function but the network can be adapted to a Cubic approximation. We note P1-KANL the KAN layer defined in [35] and its corresponding operator $\rho_{p,q}^l$ for layer l , input dimension p , output dimension q . The first layer κ^0 defined by (12) is noted ICKANL0, while a layer κ^l with $l > 0$ defined by (13) is noted ICKANL1. The structure of the network is given on (5). The recursion described in (5) is given for $M > 0$ by:

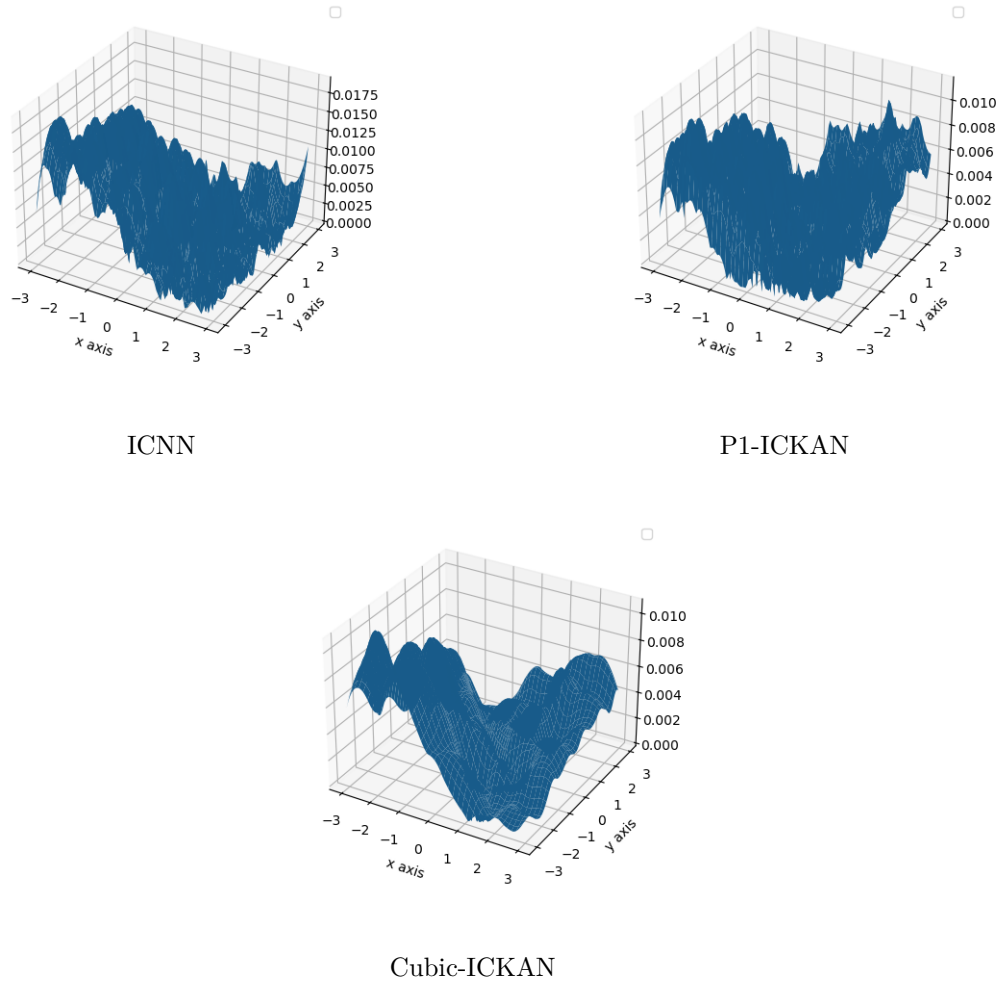


Figure 4: Relative error (21) obtained on the Linear Quadratic optimal control problem.

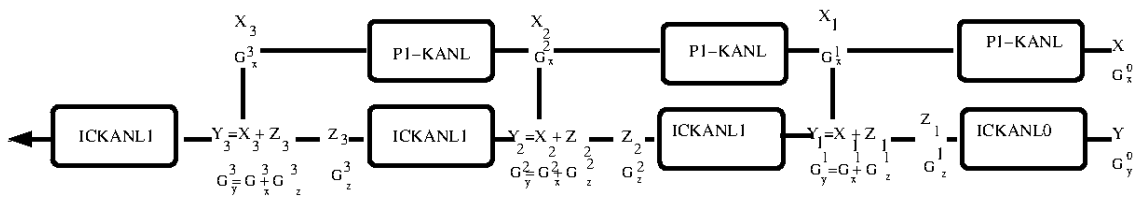


Figure 5: Partial Input Convex Kolmogorov Arnold Network using a piecewise linear approximation.

$$\begin{aligned}
(X_1, G_x^1) &= \rho_{n_x, M}^0(x, G_x^0), \\
(Y_1, G_y^1) &= (X_1, G_x^1) + \kappa_{n_y, M}^0(y, G_y^0), \\
(X_{i+1}, G_x^{i+1}) &= \rho_{M, M}^{i+1}(X_i, G_x^i), \\
(Y_{i+1}, G_y^{i+1}) &= (X_{i+1}, G_x^{i+1}) + \kappa_{M, M}^{i+1}(Y_i, G_y^i) \quad \text{for } i = 0, L-2, \\
(Y_L, G_y^L) &= \kappa_{M, 1}^L(Y_{L-1}, G_y^{L-1}).
\end{aligned}$$

remark 3.1 Notice that when f is a non convex function imposing that $\kappa^l = 0$ for $l < L$ and $\kappa^L(x) = x_1$ gives back the P1-KAN network which has a clear convergence error when the Kolmogorov Arnold basis functions are Lipschitz.

When the function f is convex, nullifying the output of the P1-KANL layers gives back the ICKAN neural network.

remark 3.2 In the PICKAN, we add the results from the convex part and the non convex part as done in the Kolmogorov Arnold layer (2).

remark 3.3 Depending on the regularity of the function in y and x , it is possible the use a scheme in x with an approximation order different from the one used in y .

remark 3.4 The PICKAN proposed here belongs to the class of Parametrized convex function considered in [26]. The architecture proposed in (5) is however different from the one proposed by Schaller et al. in [26]: they consider a feed forward neural network with layers having parameters (weights and offsets) depending on y , with a nondecreasing convex activation function and non negative weights, taking also x as an input in addition to the output of the previous layer.

We estimate the function

$$f(x, y) = |y + 1||x + 2x^3| \text{ on } [-2, 2]^2, \quad (22)$$

minimizing the empirical version of

$$\mathbb{E}[(f(X, Y) - \tilde{f}^\theta(X, Y))^2],$$

where \tilde{f}^θ is our neural network approximation parametrized by θ and $(X, Y) \sim U[-2, 2]^2$. As before we use the ADAM descent method using 200000 iterations and a learning rate equal to 10^{-3} . For the ICNN with a ReLU activation function, we use 2, 3, or 4 layers, a number of neurons in $\{10, 20, 40, 80, 160\}$. As before we compute for each configuration the averaged loss and the standard deviation obtained with 10 runs. Testing all configurations our PICNN (Partial Input Convex Neural Network in [2]) the reference is the one with the smallest averaged MSE. Results are given in (4) and show that the accuracy is again similar to the best one obtained with an ICNN. The ratio of computational time between the PICNN and the PP1-ICKAN remains consistent with results of (2.2.4).

4 Application for optimal transport

Neural networks preserving convexity can be used to solve optimal transport problems, see for example [21, 17] which use ICNN. In this section we use ICKAN models to solve optimal transport problems and compare their performance with ICNN.

Table 4: Testing partial convexity for function in (22) : average and standard deviation for 10 runs. *NBL* stands for the number of layers, *NBN* the number of neurons, *nbParam* the number of parameters of the model, while *Time* stands for the time in seconds for one hundred iterations of the stochastic gradient.

method	NBL	NBN	P	Average	std	nbParam	Time
Best PICNN	2	80		1.04E-03	7.37E-04	33126	0.28
PICKAN	2	20	20	4.98E-03	1.10E-02	18480	0.77
PICKAN	2	20	40	5.17E-03	4.87E-03	36080	0.77
PICKAN	2	40	20	2.57E-03	3.29E-03	70560	0.78
PICKAN	2	40	40	9.23E-04	5.66E-04	137760	0.78
PICKAN	3	20	20	2.10E-03	3.55E-03	35280	1.10
PICKAN	3	20	40	3.85E-03	3.69E-03	68880	1.10
PICKAN	3	40	20	3.75E-03	5.97E-03	137760	1.11
PICKAN	3	40	40	9.34E-03	1.81E-02	268960	1.11
PICKAN adapt	2	20	20	2.17E-03	2.58E-03	20120	1.05
PICKAN adapt	2	20	40	2.67E-03	4.25E-03	39360	1.05
PICKAN adapt	2	40	20	1.02E-03	1.03E-03	73800	1.06
PICKAN adapt	2	40	40	1.27E-03	1.23E-03	144240	1.06
PICKAN adapt	3	20	20	2.71E-03	3.98E-03	37720	1.48
PICKAN adapt	3	20	40	1.10E-02	1.98E-02	73760	1.48
PICKAN adapt	3	40	20	8.11E-03	1.65E-02	142600	1.49
PICKAN adapt	3	40	40	5.79E-03	5.07E-03	278640	1.49

4.1 Monge optimal transport and Brenier’s theorem

Let us consider two probability measures with support $\Omega \subset \mathbb{R}^d$, μ and ν , such that $\int_{\Omega} \|x\|^2 d\mu(x)$, $\int_{\Omega} \|x\|^2 d\nu(x) < \infty$. Our goal is to estimate the optimal transport map between X and Y , $T : \Omega \rightarrow \Omega$, which is a solution to the Monge problem [23]

$$\inf_{T\#\mu=\nu} \int_{\Omega} \|x - T(x)\|^2 d\mu(x), \quad (23)$$

where $T\#P(\cdot) := P(T^{-1}(\cdot))$ for a probability measure P and $\|\cdot\|$ denotes the Euclidean norm on \mathbb{R}^d . The Brenier’s theorem [5] guarantees the existence and uniqueness of the optimization problem in (23) as soon as the probability measure μ is absolutely continuous with respect to the \mathbb{R}^d Lebesgue measure, that we assume in the following. Furthermore, the optimal transport map T solution of the optimization problem in (23) writes $T = \nabla f$ with $f : \mathbb{R}^d \rightarrow \mathbb{R}$ a convex function differentiable almost everywhere. Furthermore, denoting $CVX(\mu)$ the set of all convex functions in $L^1(\mu)$, f is the solution of the optimization problem

$$\inf_{\varphi \in CVX(\mu)} \int_{\Omega} \varphi d\mu + \int_{\Omega} \varphi^* d\nu,$$

with $\varphi^*(y) = \sup_{x \in \Omega} \{ \langle x, y \rangle - f(x) \}$ for $y \in \Omega$ the Legendre-Fenchel transform of φ , see [22, Theorem 1]. f is called the Brenier’s potential. In [21], it is proven whenever ν admits a density, there exists an optimal pair

(φ_0, ψ_0) solution of

$$\sup_{\substack{\varphi \in CVX(\mu) \\ \varphi^* \in L^1(\nu)}} \inf_{\psi \in CVX(\nu)} - \int \varphi(x) d\mu(x) - \int (\langle y, \nabla \psi(y) \rangle - \varphi(\nabla \psi(y))) d\nu(y), \quad (24)$$

where $\nabla \psi_0 = T^{-1}$.

4.2 Algorithm

Given samples $X_1, \dots, X_n \sim \mu$ and $Y_1, \dots, Y_n \sim \nu$ both identically and independently distributed, the objective is to estimate the optimal transport map between a μ distribution and a ν distribution. We denote by $\hat{\mu}_n = \frac{1}{n} \sum_{i=1}^n \delta_{X_i}$ and $\hat{\nu}_n = \frac{1}{n} \sum_{i=1}^n \delta_{Y_i}$ the empirical distribution of X and Y respectively. In (24), the objective is to find the optimal φ and ψ that we parametrize respectively by two distinct convex neural networks φ_Θ and ψ_θ , which can be ICKAN or ICNN, $\Theta, \theta \in \mathbb{R}^l$ being the network parameters. The empirical version of (24) now solves

$$\max_{\Theta} \min_{\theta} \frac{1}{n} \sum_{i=1}^n \varphi_\Theta(\nabla \psi_\theta(Y_i)) - \langle Y_i, \nabla \psi_\theta(Y_i) \rangle - \varphi_\Theta(X_i)$$

using the classical minimax algorithm (1), where the network parameters θ are minimized in an inner loop while the other's Θ are maximized in an outer loop. Note that since the ICKAN networks are used on a

Algorithm 1 Minimax algorithm for transport problem

Require: Batch size n , external iteration I_{ext} , internal iteration I_{int} .

```

for  $i = 1, \dots, I_{ext}$  do
  for  $j = 1, \dots, I_{int}$  do
    Sample  $Y_1, \dots, Y_n \sim \nu$ 
     $\theta \leftarrow \operatorname{argmin}_{\theta} \frac{1}{n} \sum_{i=1}^n \varphi_\Theta(\nabla \psi_\theta(Y_i)) - \langle Y_i, \nabla \psi_\theta(Y_i) \rangle$  using Adam method
  end for
  Sample  $X_1, \dots, X_n \sim \mu$ 
  Sample  $Y_1, \dots, Y_n \sim \nu$ 
   $\Theta \leftarrow \operatorname{argmax}_{\Theta} \frac{1}{n} \sum_{i=1}^n \varphi_\Theta(\nabla \psi_\theta(Y_i)) - \langle Y_i, \nabla \psi_\theta(Y_i) \rangle - \varphi_\Theta(X_i)$  using Adam method
end for

```

compact set, and since we cannot control the values taken by $\nabla \psi(y)$ during the resolution, the ψ_θ network linearly extrapolates the function outside its domain of definition.

4.3 Numerical results on synthetic data

Since it is often difficult to get the transport map for a pair (ν, μ) , we define three examples using μ and T , and we consider $\nu = T\#\mu$. The metric we consider for the error between the optimal transport map T^* and the estimated one \hat{T} is the percentage of unexplained variance [17] $\text{UVP} (\%) = 100 \frac{\int_{\Omega} \|T^* - \hat{T}\|^2 d\hat{\mu}_n}{\int_{\Omega} \|x\|^2 d\hat{\nu}_n - \int_{\Omega} x d\hat{\nu}_n \|^2}$ on a validation set X_1, \dots, X_n and Y_1, \dots, Y_n (an error of 100% corresponds to the constant map $T^{\hat{C}}(x) = \int_{\Omega} x d\hat{\nu}_n(x)$). As in [17], we choose as benchmark the linear transport map estimated on the validation set defined by

$\hat{T}^L(x) = \hat{A}(x - \hat{m}_1) + \hat{m}_2$ where $\hat{m}_1 = \int_{\Omega} x d\hat{\mu}_n(x)$, $\hat{m}_2 = \int_{\Omega} x d\hat{\nu}_n(x)$, $\hat{A} = \hat{\Sigma}_1^{-1/2} \left(\hat{\Sigma}_1^{1/2} \hat{\Sigma}_2 \hat{\Sigma}_1^{1/2} \right)^{1/2} \hat{\Sigma}_1^{-1/2}$, $\hat{\Sigma}_1 = \int_{\Omega} x x^{\top} d\hat{\mu}_n(x) - \hat{m}_1 \hat{m}_1^{\top}$ and $\hat{\Sigma}_2 = \int_{\Omega} x x^{\top} d\hat{\nu}_n(x) - \hat{m}_2 \hat{m}_2^{\top}$ assumed positive definite, see [10]. We consider for the optimization the same hyperparameters than [17], that is

- $I_{ext} = 50000$ iterations and $I_{int} = 15$ iterations ;
- at each iteration, we simulate a new batch of size 1024 ;
- the learning rate is equal to 0.001 ;
- every 100 iterations, we evaluate the error UVP on a test set consisting of 4096 data and we keep the network with the lowest error ;
- the validation dataset has size 2^{14} .

For the ICKAN networks, the domain is defined from the minimum and maximum values from a first dataset with 2^{14} data. This framework is idealised, as in practice we by no means have this amount of data and we do not have access to the optimal map used in to evaluate the error for the test set. We also initialise the networks with θ_0 minimising $\|\nabla f_{\theta}(x) - x\|^2$ so that the map is closed to identity at initialisation.

Transport map of [17] We consider the transport map defined in the work of Korotin et al. [17]: the authors consider the optimal transport map T_1 between a mixture of 3 Gaussian random variables μ and a mixture of 10 Gaussian random variables and the optimal transport map T_2 between the same mixture of 3 Gaussian random variables and another mixture of 10 Gaussian random variables. They can then define the optimal transport map $\frac{1}{2}(T_1 + T_2)$. Since T_1 and T_2 are not explicitly known, they learn T_1 and T_2 with an ICNN, \hat{T}_1 and \hat{T}_2 respectively, that solves the optimal transport problem. The target distribution considered by Korotin et al. [17] and by us is then $\frac{1}{2}(\hat{T}_1 + \hat{T}_2) \# \mu$. We consider for the ICNN¹ 3 layers with 64, 64 and 32 neurons (same parametrisation as in [17]) and for the ICKANs a network with 2 layers with 64 and 32 neurons or with 10 and 5 neurons. The results are given in (5) for $d \in \{2, 4, 4, 8, 16, 32\}$. Our optimization framework and network parametrization correspond to the [MMv2] case in [17]. For the Cubic ICKAN with adapted mesh and with 64 and 32 neurons, the errors are much smaller than for the linear map, but can be slightly larger than those obtained by the ICNN parametrization in some case, with similar orders of magnitude. As mentioned in [17], the optimal transport map itself is learned with an ICNN, which can be advantageous for the ICNN parametrisation. Furthermore, we did not search for the optimal parametrisation of the Cubic ICKAN (nor for the ICNN). The number of mesh points $P \in \{10, 20, 40\}$ does not have much influence on the results, as the use of an unadapted grid does. However, using a P1 mesh instead of a cubic one significantly degrades the results, but the network still outperforms the linear map. Using a smaller network of 10 and 5 neurons for the Cubic ICKAN results in larger errors, and this difference increases with dimension. The obtained distributions are displayed in (6) for the case $d = 2$ and the Cubic ICKAN with $P = 10$.

¹We use the implementation at <https://github.com/iamalexkorotin/Wasserstein2Benchmark/>, which uses a CELU activation function.

Table 5: Percentage of unexplained variance UVP (%) for the linear map, the map parametrized by the Cubic ICKAN with adapted mesh and $P \in \{10, 20, 40\}$, the Cubic ICKAN with non adapted mesh and $P = 40$, the P1-ICKAN with adapted mesh and $P = 40$ and the ICNN map when the true map is the one in [17]. For the Cubic ICKAN, we consider networks with 2 layers and 64 and 32 neurons or 10 and 5 neurons, for the P1-ICKAN 2 layers with 64 and 32 neurons, while for the ICNN we consider 3 layers with 64, 64, and 32 neurons.

Method	Neurons / Dim	2	4	8	16	32
Linear		13.93	14.96	27.29	42.05	55.48
Cubic ICKAN P=10 adapt	64 32	0.06	0.58	3.00	7.16	9.89
Cubic ICKAN P=20 adapt	64 32	0.05	0.51	2.44	5.97	7.66
Cubic ICKAN P=40 adapt	64 32	0.05	0.52	2.82	6.57	5.90
Cubic ICKAN P=40	64 32	0.06	0.65	3.66	6.63	10.98
P1-ICKAN P=40 adapt	64 32	1.01	6.62	19.99	19.90	27.95
Cubic ICKAN P=40 adapt	10 5	0.16	1.84	11.56	47.25	101.83
ICNN	64 64 32	0.07	0.27	0.74	1.98	3.01

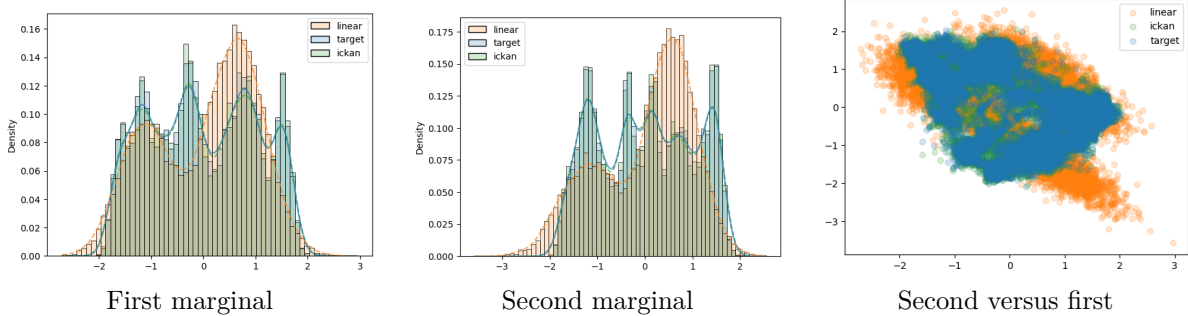


Figure 6: Distribution of the true target distribution as well as the one obtained by linear transport or Cubic ICKAN transport with adapted mesh, $P = 10$, and 64 and 32 neurons for the map in [17] and $d = 2$. The first two figures include the empirical histogram as well as a Gaussian kernel density estimator with bandwidth selected using Scott's rule [27] (solid line for target, dashed lines for linear and ICKAN transports).

Tensorized case [32] We consider the example in Vacher et al. [32] where the transport map is defined by $T(x) = (T_i(x_i))_{i=1,\dots,d}$ with $T_i(x_i) = x_i + \frac{1}{6-\cos(2\pi x_i)} - 0.2$, $i = 1, \dots, d$,² for $x = (x_i)_{i=1,\dots,d} \in [0, 1]^d$. μ is a uniform law on $[0, 1]^d$. We consider a 3-layers ICNN with 64, 64, 32 neurons and a 2-layers Cubic ICKAN with $\max(2d, 10)$ and $\max(d, 5)$ neurons, an adapted mesh and $P \in \{10, 20, 40\}$. The results are given in (6) for $d \in \{1, 2, 4, 8\}$. The ICNN performs very poorly for $d \in \{4, 8\}$, giving errors of the same order of magnitude as the linear transport map. The Cubic ICKAN performs very well for all values of P . The obtained distributions are displayed in (7) for the case $d = 2$ case and the Cubic ICKAN with $P = 10$. We also display in (8) the first component of $\hat{T}((x \ 0.5)^\top)$ (0.5 is chosen arbitrarily, the first component of $x_2 \rightarrow \hat{T}((x \ x_2)^\top)$ being constant and estimating $T_1(x)$), and the second component of $\hat{T}((0.5 \ x)^\top)$. We get similar figures for larger dimensions. The neural network reproduces the target distribution and the transport map very well. The better performance of ICKAN over ICNN is probably due to the structure of the Brenier map, which is of the form $f(x) = \sum_{i=1}^d f_i(x_i)$ with $f_i(x_i) = \int_0^{x_i} T_i(s) ds$, $i = 1, \dots, d$: the functions in the Arnold-Kolmogorov representation (3) then have a high degree of smoothness which can lead to a faster rate of convergence, see Proposition 2.2 and 2.3 in [35] in the non-convex case.

Table 6: Percentage of unexplained variance UVP (%) for the linear map, the map parametrized by the Cubic ICKAN with adapted mesh and $P \in \{10, 20, 40\}$, and the ICNN map and different dimensions when the true map is $T(x) = (T_i(x_i))_{i=1,\dots,d}$ with $T_i(x_i) = x_i + \frac{1}{6-\cos(2\pi x_i)} - 0.2$, $i = 1, \dots, d$.

Method / Dim	1	2	4	8
Linear	0.49	0.54	0.52	0.53
Cubic ICKAN P=10	0.00	0.01	0.01	0.02
Cubic ICKAN P=20	0.00	0.02	0.02	0.02
Cubic ICKAN P=40	0.01	0.02	0.02	0.02
ICNN	0.04	0.05	0.34	0.51

Product case In this last case, we consider the map $T = \nabla f$ with f the convex function defined on $[0, 1]^d$ by

$$f(x) = 3^{-d} \prod_{i=1}^d (x_i^2 + x_i + 1), \quad (25)$$

and μ is the uniform law on $[0, 1]^d$. The networks have the same architecture as in the second case (tensorized map). The results are given in (7): ICKAN and ICNN give similar results and outperform the linear map benchmark (except for the case $d = 1$ where the optimal transport map is linear).

5 Conclusion

Depending on the case, the new Kolmogorov-Arnold network may outperform the ICNN, though this depends heavily on the case. Therefore, this new network may provide an alternative to the ICNN, depending on the structure of the solution. One obvious example is when the solution is separable, as demonstrated

²The example considered is the one from the code <https://github.com/litlboy/OT-Model-Selection/blob/main/Synth-XP/Tensorised/sinkhorn.py> which differs from the one of the paper [32].

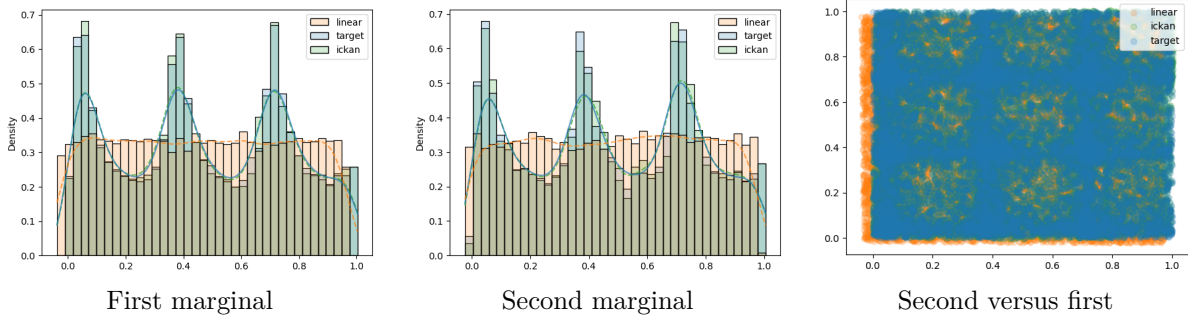


Figure 7: Distribution of the true target distribution as well as the one obtained by linear transport or Cubic ICKAN transport with adapted mesh and $P = 10$, for the map $T(x) = (T_i(x_i))_{i=1,2}$ with $T_i(x_i) = x_i + \frac{1}{6 - \cos(2\pi x_i)} - 0.2$, $i = 1, 2$. The first two figures include the empirical histogram as well as a Gaussian kernel density estimator with bandwidth selected using Scott's rule [27] (solid line for target, dashed lines for linear and ICKAN transports).

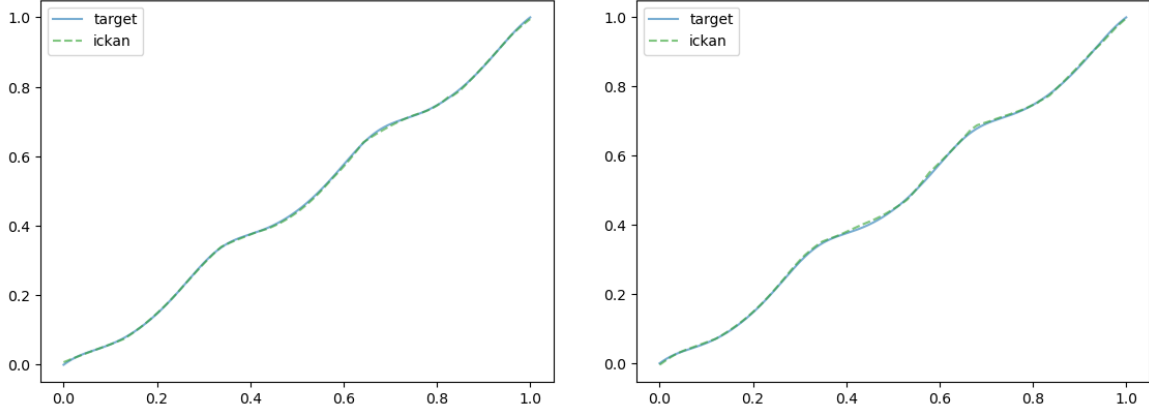


Figure 8: $x \mapsto T_1(x)$ (left) and $x \mapsto T_2(x)$ (right) for the map $T(x) = (T_i(x_i))_{i=1,2}$ with $T_i(x_i) = x_i + \frac{1}{6 - \cos(2\pi x_i)} - 0.2$, $i = 1, 2$ as well as the first component of $x \mapsto \hat{T}((x \ 0.5)^\top)$ (left) and the second component of $x \mapsto \hat{T}((0.5 \ x)^\top)$ with \hat{T} the estimated map parametrized by the Cubic ICKAN with adapted mesh and $P = 10$.

Table 7: Percentage of unexplained variance UVP (%) for the linear map, the map parametrized by the Cubic ICKAN with adapted mesh and $P = 40$, and the ICNN map and different dimensions when the true map is $T(x) = \nabla f(x)$ with f given in (25).

Method / Dim	1	2	4	8
Linear	0.00	6.90	16.43	33.57
Cubic ICKAN P=40	0.01	3.15	2.33	2.85
ICNN	0.00	2.77	1.81	1.30

in (4). Additionally, Kolmogorov-Arnold networks are known to be more interpretable than multilayer perceptrons (MLPs) as they are compositions of one-dimensional functions that can easily be plotted, a feature appreciated by users needing to explain the obtained results. Similarly to the original spline KAN that saw its computational cost highly reduced using an implementation different from the original design³, more effective implementation of the ICKAN may be possible and is left to future research.

³<https://github.com/Blealtan/efficient-KAN>

References

- [1] Akshay Agrawal, Shane Barratt, Stephen Boyd, and Bartolomeo Stellato. Learning convex optimization control policies. In Learning for Dynamics and Control, pages 361–373. PMLR, 2020.
- [2] Brandon Amos, Lei Xu, and J Zico Kolter. Input convex neural networks. In International conference on machine learning, pages 146–155. PMLR, 2017.
- [3] Gábor Balázs, András György, and Csaba Szepesvári. Near-optimal max-affine estimators for convex regression. In Artificial Intelligence and Statistics, pages 56–64. PMLR, 2015.
- [4] Zavareh Bozorgasl and Hao Chen. Wav-Kan: Wavelet Kolmogorov-Arnold Networks. arXiv preprint arXiv:2405.12832, 2024.
- [5] Yann Brenier. Polar factorization and monotone rearrangement of vector-valued functions. Communications on pure and applied mathematics, 44(4):375–417, 1991.
- [6] Giuseppe C Calafiore, Stephane Gaubert, and Corrado Possieri. Log-sum-exp neural networks and posynomial models for convex and log-log-convex data. IEEE transactions on neural networks and learning systems, 31(3):827–838, 2019.
- [7] Yize Chen, Yuanyuan Shi, and Baosen Zhang. Optimal control via neural networks: A convex approach. arXiv preprint arXiv:1805.11835, 2018.
- [8] Yize Chen, Yuanyuan Shi, and Baosen Zhang. Input convex neural networks for optimal voltage regulation. arXiv preprint arXiv:2002.08684, 2020.
- [9] Robert Demb and David Sprecher. A note on computing with Kolmogorov superpositions without iterations. Neural Networks, 144:438–442, 2021.
- [10] Rémi Flamary, Karim Lounici, and André Ferrari. Concentration bounds for linear Monge mapping estimation and optimal transport domain adaptation. arXiv preprint arXiv:1905.10155, 2019.
- [11] Avishek Ghosh, Ashwin Pananjady, Adityanand Guntuboyina, and Kannan Ramchandran. Max-affine regression: Provable, tractable, and near-optimal statistical estimation. arXiv preprint arXiv:1906.09255, 2019.
- [12] Avishek Ghosh, Ashwin Pananjady, Adityanand Guntuboyina, and Kannan Ramchandran. Max-affine regression: Parameter estimation for gaussian designs. IEEE Transactions on Information Theory, 68(3):1851–1885, 2021.
- [13] Federico Girosi and Tomaso Poggio. Representation properties of networks: Kolmogorov’s theorem is irrelevant. Neural Computation, 1(4):465–469, 1989.
- [14] Seonho Kim and Kiryung Lee. Max-affine regression via first-order methods. SIAM Journal on Mathematics of Data Science, 6(2):534–552, 2024.
- [15] Andrei Nikolaevich Kolmogorov. On the representation of continuous functions of several variables by superpositions of continuous functions of a smaller number of variables. American Mathematical Society, 1961.

- [16] Alexander Korotin, Vage Egiazarian, Arip Asadulaev, Alexander Safin, and Evgeny Burnaev. Wasserstein-2 generative networks. [arXiv preprint arXiv:1909.13082](#), 2019.
- [17] Alexander Korotin, Lingxiao Li, Aude Genevay, Justin M Solomon, Alexander Filippov, and Evgeny Burnaev. Do neural optimal transport solvers work? A continuous Wasserstein-2 benchmark. [Advances in neural information processing systems](#), 34:14593–14605, 2021.
- [18] Věra Kůrková. Kolmogorov’s theorem and multilayer neural networks. [Neural networks](#), 5(3):501–506, 1992.
- [19] Ziyao Li. Kolmogorov-Arnold Networks are Radial Basis Function Networks. [arXiv preprint arXiv:2405.06721](#), 2024.
- [20] Ziming Liu, Yixuan Wang, Sachin Vaidya, Fabian Ruelle, James Halverson, Marin Soljačić, Thomas Y Hou, and Max Tegmark. KAN: Kolmogorov-Arnold Networks. [arXiv preprint arXiv:2404.19756](#), 2024.
- [21] Ashok Makkuva, Amirhossein Taghvaei, Sewoong Oh, and Jason Lee. Optimal transport mapping via input convex neural networks. In [International Conference on Machine Learning](#), pages 6672–6681. PMLR, 2020.
- [22] Tudor Manole, Sivaraman Balakrishnan, Jonathan Niles-Weed, and Larry Wasserman. Plugin estimation of smooth optimal transport maps. [The Annals of Statistics](#), 52(3):966–998, 2024.
- [23] Gaspard Monge. Mémoire sur la théorie des déblais et des remblais. [Mem. Math. Phys. Acad. Royale Sci.](#), pages 666–704, 1781.
- [24] Subhadip Mukherjee, Sören Dittmer, Zakhar Shumaylov, Sebastian Lunz, Ozan Öktem, and Carola-Bibiane Schönlieb. Learned convex regularizers for inverse problems. [arXiv preprint arXiv:2008.02839](#), 2020.
- [25] Tomaso Poggio, Andrzej Banburski, and Qianli Liao. Theoretical issues in deep networks. [Proceedings of the National Academy of Sciences](#), 117(48):30039–30045, 2020.
- [26] Maximilian Schaller, Alberto Bemporad, and Stephen Boyd. Learning parametric convex functions. [arXiv preprint arXiv:2506.04183](#), 2025.
- [27] David W. Scott and Stephan R. Sain. 9 - Multidimensional Density Estimation. In C.R. Rao, E.J. Wegman, and J.L. Solka, editors, [Data Mining and Data Visualization](#), volume 24 of [Handbook of Statistics](#), pages 229–261. Elsevier, 2005.
- [28] S. S. Sidharth, A. R. Keerthana, R. Gokul, and K. P. Anas. Chebyshev polynomial-based Kolmogorov–Arnold networks: An efficient architecture for nonlinear function approximation. [arXiv preprint arXiv:2405.07200](#), 2024.
- [29] Lunji Song, Juan Diego Toscano, and Li-Lian Wang. Explicit construction of approximate Kolmogorov-Arnold superpositions with C2-smoothness. [arXiv preprint arXiv:2508.04392](#), 2025.
- [30] Hoang-Thang Ta. BSRBF-KAN: A combination of B-splines and Radial Basic Functions in Kolmogorov-Arnold Networks. [arXiv preprint arXiv:2406.11173](#), 2024.

- [31] Prakash Thakolkaran, Yaqi Guo, Shivam Saini, Mathias Peirlinck, Benjamin Alheit, and Siddhant Kumar. Can KAN CANs? Input-convex Kolmogorov-Arnold networks (KANs) as hyperelastic constitutive artificial neural networks (CANs). Computer Methods in Applied Mechanics and Engineering, 443:118089, 2025.
- [32] Adrien Vacher and François-Xavier Vialard. Parameter tuning and model selection in optimal transport with semi-dual Brenier formulation. Advances in Neural Information Processing Systems, 35:23098–23108, 2022.
- [33] Xavier Warin. Some non-monotone schemes for time dependent hamilton–jacobi–bellman equations in stochastic control. Journal of Scientific Computing, 66(3):1122–1147, 2016.
- [34] Xavier Warin. The GroupMax neural network approximation of convex functions. IEEE Transactions on Neural Networks and Learning Systems, 2023.
- [35] Xavier Warin. P1-KAN: an effective Kolmogorov-Arnold Network with application to hydraulic valley optimization. arXiv preprint arXiv:2410.03801, 2024.

A One dimensional approximation with one layer

For the P1-ICKAN and the Cubic-ICKAN, we show the 1 layer approximation of some convex functions using adaptation.

A.1 Using P1-ICKAN

As an example, it is possible to minimize the mean squared error of a one dimensional convex function with its approximation (4)-(6) training $b, \hat{b}, (d_i)_{i=1, \dots, P-1}$, and $(e_i)_{i=1, \dots, P}$. With θ the vector of parameters to be trained, our approximation \tilde{f}^θ of a function f is parametrized by θ and we minimize

$$\mathbb{E}[(f(X) - \tilde{f}^\theta(X))^2]$$

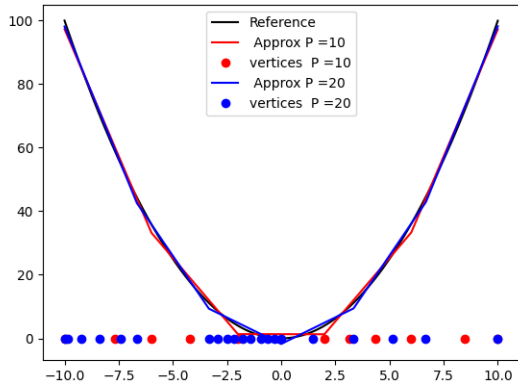
where X is a random variable sampled uniformly on $[-10, 10]$. We give the results approximating the functions $f_i, i = 1, \dots, 4$ on (9) where

1. $f_1(x) = x^2$,
2. $f_2(x) = x^2 + 10[(e^x - 1)1_{x < 0} + x1_{x \geq 0}]$,
3. $f_3(x) = (|x|^2 + 1)^2$,
4. $f_4(x) = |x|1_{|x| \leq 3} + \frac{x^2 - 3}{2}$.

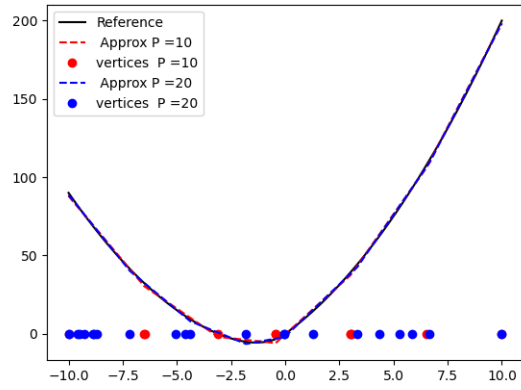
The plots are obtained adapting the grid with $P = 10$ or $P = 20$. We also plot the adapted vertices.

A.2 Cubic-ICKAN

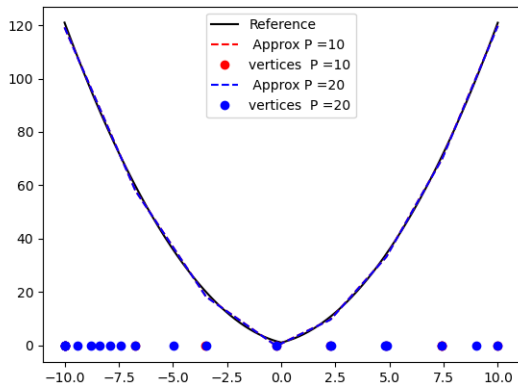
As for the piecewise linear approximation we provide on (10) the vertices and an estimation obtained adapting the grid with $P = 5$ or $P = 10$.



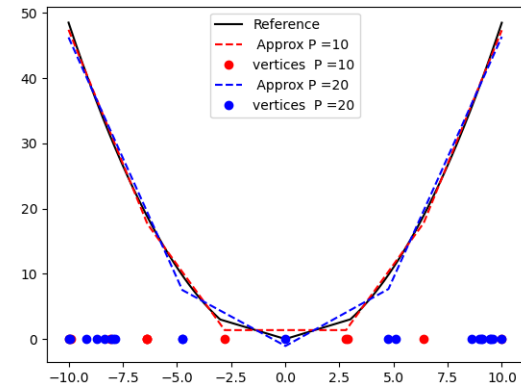
f_1



f_2



f_3



f_4

Figure 9: Piecewise linear approximation of a one dimensional function using (4)- (6) with adaptation.

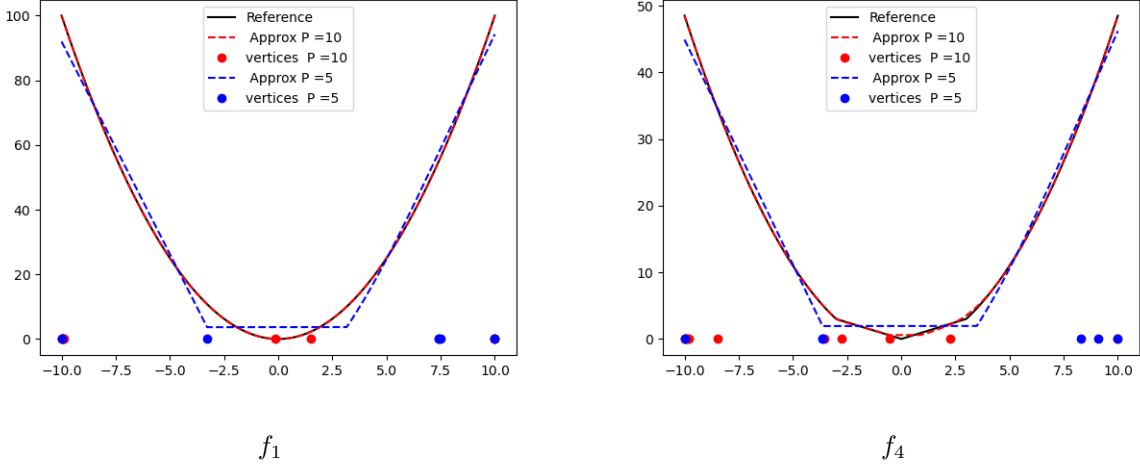


Figure 10: Cubic spline approximation of a one dimensional function using (8)- (9) with adaptation.

B Proof of (2.1) and (2.2)

B.1 Proof of (2.1)

The proof is constructive and is based on proof of theorem 1 in [7]. One wants to approximate a Lipschitz convex function on $[0, 1]^n$ denoted f by a P1-ICKAN network with adaptation. First any Lipschitz convex function on $[0, 1]^n$ can be approximated within ϵ by the maximum of a finite set of affine functions (Lemma 1 in [7] or Proposition 1 in [34]), that is for $\epsilon > 0$, there exists $N \geq 1$ and a function f_N such that $|f(x) - f_N(x)| < \epsilon$ for any $x \in [0, 1]^n$, having representation

$$f_N(x) := \max(\alpha_1^\top x + \beta_1, \dots, \alpha_N^\top x + \beta_N), \quad \alpha_i \in \mathbb{R}^n, \beta_i \in \mathbb{R}, i = 1, \dots, N. \quad (26)$$

As a consequence, the proof of (2.1) boils down to show that the P1-ICKAN network with adaptation can represent any maximum of a finite set of affine functions of type (26) for any $N \geq 1$.

Following [7], we start by the case $N = 2$ and begin to show that the linear KAN can represent the maximum of two affine functions, that is any function of the form f_2 . First, we have for $x \in [0, 1]^n$, $\alpha_i \in \mathbb{R}^n$, $\beta_i \in \mathbb{R}$, $i = 1, 2$,

$$f_2(x) = \max((\alpha_1^\top - \alpha_2^\top)x + \beta_1 - \beta_2, 0) + \alpha_2^\top x + \beta_2. \quad (27)$$

We consider $P = 2$ and a $L = 3$ -layers neural network to equalize (27) with $n_1 = 3$ neurons for the first layer and $n_2 = 2$ neurons for the second layer. For the first layer, we consider the lattice defined by $\hat{x}_{0,j,0} = 0$,

$\hat{x}_{0,j,1} = \frac{1}{2}$, and $\hat{x}_{0,j,2} = 1$, $1 \leq j \leq n$, and we define in (10) the parameters

$$\begin{aligned}
b_{0,1,1} &= \beta_1, \\
b_{0,1,j} &= 0 \text{ for } 1 < j \leq n, \\
\hat{b}_{0,1,j} &= \alpha_{1,j} \text{ for } 1 \leq j \leq n, \\
d_{0,1,j,1} &= 0 \text{ for } 1 \leq j \leq n, \\
b_{0,2,1} &= -\beta_2, \\
b_{0,2,j} &= 0 \text{ for } 1 < j \leq n, \\
\hat{b}_{0,2,j} &= -\alpha_{2,j} \text{ for } 1 \leq j \leq n, \\
d_{0,2,j,1} &= 0 \text{ for } 1 \leq j \leq n, \\
b_{0,3,1} &= \beta_2, \\
b_{0,3,j} &= 0 \text{ for } 1 < j \leq n, \\
\hat{b}_{0,3,j} &= \alpha_{2,j} \text{ for } 1 \leq j \leq n, \\
d_{0,3,j,1} &= 0 \text{ for } 1 \leq j \leq n.
\end{aligned} \tag{28}$$

One checks that the output of the first layer is given by

$$\begin{aligned}
\hat{\kappa}_{n,n_1}^0(x, [0, 1]^n)_1 &= \alpha_1^\top x + \beta_1, \\
\hat{\kappa}_{n,n_1}^0(x, [0, 1]^n)_2 &= -\alpha_2^\top x - \beta_2, \\
\hat{\kappa}_{n,n_1}^0(x, [0, 1]^n)_3 &= \alpha_2^\top x + \beta_2.
\end{aligned}$$

For the second layer, we have $n_2 = 2$ neurons. Let $I_1 = \prod_{j=1}^3 [\hat{x}_{1,j,0}, \hat{x}_{1,j,2}]$ denote the image of $[0, 1]^n$ by the first layer and consider for each $j = 1, 2, 3$ any $\hat{x}_{1,j,1} \in]\hat{x}_{1,j,0}, \hat{x}_{1,j,2}[$ to define the grid \mathcal{G}^1 . For the first neuron, we consider the parameters

$$\begin{aligned}
b_{1,1,j} &= \hat{x}_{1,j,0}, \quad j = 1, 2, \\
\hat{b}_{1,1,j} &= 1, \quad j = 1, 2, \\
d_{1,1,j,1} &= 0, \quad j = 1, 2, \\
b_{1,1,3} &= 0, \\
\hat{b}_{1,1,3} &= 0, \\
d_{1,1,3,1} &= 0
\end{aligned}$$

in order to get

$$\hat{\kappa}_{n_1,n_2}^1(x, \mathcal{G}_1)_1 = x_1 + x_2.$$

In the same way, for the second neuron, we consider the parameters

$$\begin{aligned}
b_{1,2,j} &= 0, \quad j = 1, 2, \\
\hat{b}_{1,2,j} &= 0, \quad j = 1, 2, \\
d_{1,2,j,1} &= 0, \quad j = 1, 2, \\
b_{1,2,3} &= \hat{x}_{1,3,0}, \\
\hat{b}_{1,2,3} &= 1, \\
d_{1,2,3,1} &= 0
\end{aligned}$$

to get

$$\hat{\kappa}_{n_1, n_2}^1(x, \mathcal{G}_1)_2 = x_3.$$

At this stage, we then have as output of the two first layers

$$\begin{aligned}
\hat{\kappa}_{n_1, n_2}^1 \circ \kappa_{n, n_1}^0(x, [0, 1]^n)_1 &= (\alpha_1^\top - \alpha_2^\top)x + \beta_1 - \beta_2, \\
\hat{\kappa}_{n_1, n_2}^1 \circ \kappa_{n, n_2}^0(x, [0, 1]^n)_2 &= \alpha_2^\top x + \beta_2.
\end{aligned}$$

Let $I_2 = \prod_{j=1}^2 [\hat{x}_{2,j,0}, \hat{x}_{2,j,2}]$ denote the image of \mathcal{G}_1 by the second layer. For the third layer, we first consider the case where the non linearity is active for the first component of the second layer output $\hat{\kappa}_{n_1, n_2}^1 \circ \kappa_{n, n_1}^0(x, [0, 1]^n)_1$, that is $0 \in]\hat{x}_{2,1,0}, \hat{x}_{2,1,2}[$ (only depending on the function that we try to equalize, f_2). In this case, we take $\hat{x}_{2,1,1} = 0 \in]\hat{x}_{2,1,0}, \hat{x}_{2,1,2}[$, and any $\hat{x}_{2,2,1} \in]\hat{x}_{2,2,0}, \hat{x}_{2,2,2}[$ to construct \mathcal{G}_2 , and define

$$\begin{aligned}
b_{2,1,1} &= 0, \\
\hat{b}_{2,1,1} &= 0, \\
d_{2,1,1,1} &= 1, \\
b_{2,1,2} &= \hat{x}_{2,2,0}, \\
\hat{b}_{2,1,2} &= 1, \\
d_{2,1,2,1} &= 0.
\end{aligned} \tag{29}$$

The three first lines in (29) define the ReLU with an active non linearity, while the three last define the identity function. We thus get the desired result

$$\hat{\kappa}_{n_2, 1}^1 \circ \kappa_{n_1, n_2}^1 \circ \kappa_{n, n_1}^0(x, [0, 1]^n)_1 = \max((\alpha_1^\top - \alpha_2^\top)x + \beta_1 - \beta_2, 0) + \alpha_2^\top x + \beta_2$$

equal to $f_2(x)$ from (27). Now consider the case when the non linearity is not active. It is enough to take for the lattice any $\hat{x}_{2,1,1} \in]\hat{x}_{2,1,0}, \hat{x}_{2,1,2}[$ and to replace $b_{2,1,1}$, $\hat{b}_{2,1,1}$, and $d_{2,1,1,1}$ in (29) by

$$\begin{aligned}
b_{2,1,1} &= \hat{x}_{2,1,0}, \\
\hat{b}_{2,1,1} &= 1, \\
d_{2,1,1,1} &= 0
\end{aligned}$$

to obtain the identity function.

Similarly as in [7], one can extend iteratively the procedure for a given N using

$$f_N(x) = \max(f_{N-1}(x) - (\alpha_N^\top x + \beta_N), 0) + \alpha_N^\top x + \beta_N. \quad (30)$$

If one has constructed $f_{N-1}(x)$, add

- Two neurons at the end of the first layer, with outputs $-\alpha_N^\top x - \beta_N$ and $\alpha_N^\top x + \beta_N$, in the same way as the last two neurons in the first layer in the case $N = 2$,
- Two neurons at the end of each existing layer, that output exactly the outputs of the two last neurons of the previous layer, in the same way that the last neuron in the second layer in the case $N = 2$, and we get $-\alpha_N^\top x - \beta_N$ and $\alpha_N^\top x + \beta_N$ for the outputs of the two last neurons of the last layer.

From this, we get a third dimensional output corresponding to $f_{N-1}(x)$, $-\alpha_N^\top x - \beta_N$ and $\alpha_N^\top x + \beta_N$. The situation is exactly the same as for the case $N = 2$, after that the first layer has been constructed. It remains to add the two layers similar to the two last layers in the case $N = 2$ to get the desired output (30).

remark B.1 *The first layer outputs $-\alpha_N^\top x - \beta_N$ in order to avoid to have negative values of $\hat{b}_{l,k,j}$ in the other layers which, contrarily to the first layer, consider $\max(\hat{b}_{l,k,j}, 0)$ and not $\hat{b}_{l,k,j}$. This is similar to the duplication trick in the proof of theorem 1 in [7].*

B.2 Proof of (2.2)

The idea of the proof is the same as in the adapted case. For sake of simplicity, we allow here the number of mesh points $P + 1$ to vary from one neuron to another, which changes nothing as a neuron with mesh size $M + 1$ is a particular case of a neuron with mesh size $P + 1$ if $M \leq P$. Consider first the case $N = 2$ as in the proof of the adapted case. The two first layers are designed similarly. On the third layer, only the case where the non linearity is active differs. Notice that, a priori, $0 \notin]\hat{x}_{2,1,0}, \hat{x}_{2,1,2}[$. Then using a given P value for this layer for the first neuron, we can find k such that $|\hat{x}_{2,1,k}| \leq \frac{\hat{x}_{2,1,P} - \hat{x}_{2,1,0}}{P}$. Take

$$\begin{aligned} b_{2,1,1} &= 0, \\ \hat{b}_{2,1,1} &= 0, \\ d_{2,1,1,i} &= 0, \text{ for } i \neq k \\ d_{2,1,1,k} &= 1 \end{aligned}$$

and we keep $P = 2$ for the second neuron and parameters

$$\begin{aligned} b_{2,1,2} &= \hat{x}_{2,2,0}, \\ \hat{b}_{2,1,2} &= 1, \\ d_{2,1,2,1} &= 0. \end{aligned}$$

Then we get for the output of the neural network

$$\begin{aligned} \kappa_2(x) &:= \hat{\kappa}_{n_2,1}^1 \circ \kappa_{n_1,n_2}^1 \circ \kappa_{n,n_1}^0(x, [0, 1]^n)_1 \\ &= \max((\alpha_1^\top - \alpha_2^\top)x + \beta_1 - \beta_2 - \hat{x}_{2,1,k}, 0) + \alpha_2^\top x + \beta_2 \end{aligned}$$

so that

$$|f_2(x) - \kappa_2(x)| \leq |\hat{x}_{2,1,k}| \leq \frac{C_2}{P}.$$

The previous result can be extended to the general case $N \geq 2$ so that our network representation κ_N is such that

$$|f_N(x) - \kappa_N(x)| \leq \frac{C_N}{P}$$

and

$$|f(x) - \kappa_N(x)| \leq \frac{C_N}{P} + \epsilon.$$

Therefore, setting P equal to the integer part of $\frac{C_N}{\epsilon} + 1$ provides a 2ϵ approximation of f .